Origin of anomalous values of $\sigma(\pi^+,\pi^{+\prime}p)/\sigma(\pi^-,\pi^{-\prime}p)$

Dean Halderson
Department of Physics, Western Michigan University, Kalamazoo, Michigan 49008

V. A. Sadovnikova
Petersburg Nuclear Physics Institute, Russian Academy of Sciences, Gatchina, 188350 Russia

(Received 11 April 1997)

Results of recoil-corrected continuum shell model calculations are presented for ^{4}He$(\pi,\pi'p)^3$H. The extremely large values of $\sigma(\pi^+,\pi^{+\prime}p)/\sigma(\pi^-,\pi^{-\prime}p)$ are shown to be a result of neutron excitations which couple to outgoing proton channels. The large ratio will occur in regions where neutron excitations increase rapidly in a particular channel and, therefore, may be a signal for giant resonances. [S0556-2813(97)05011-5]

PACS number(s): 25.80.Hp, 14.20.Gk, 24.30.Cz, 27.10.+h

I. INTRODUCTION

Although often considered a simple nuclear system with excited states, ^{4}He has exhibited unexpected behavior. For instance, some measurements of $\sigma(\gamma,n)/\sigma(\gamma,p)$ cross section ratios with both real and virtual photons showed significant discrepancies with theoretical predictions [1]. Only the addition of large isospin symmetry-breaking components to the NN interaction could reproduce $\sigma(\gamma,n)/\sigma(\gamma,p)$ ratios different than unity [2].

Efforts to investigate isospin-violating processes in ^{4}He have uncovered another unexpected result. Exclusive measurements of $(\pi,\pi'p)$ have yielded $(\pi^+,\pi^{+\prime}p)/(\pi^-,\pi^{-\prime}p)$ cross section ratios ranging from 0.2 to 50 [3,4]. In a quasifree model of pion scattering in the Δ_{33} resonance region, exclusive $(\pi,\pi'p)$ cross sections should yield a $(\pi^+,\pi^{+\prime}p)/(\pi^-,\pi^{-\prime}p)$ ratio of approximately 9. Indeed, quasifree codes [5] with distortion effects produce little variation from this ratio of 9 [3].

A similar ratio of 40 was observed in ^{16}O at $\theta_\pi=35°$ for $T_\pi=240$ MeV [6]. In Ref. [6] calculations for ^{16}O were performed in the Δ-hole formalism with rescattering. Within the flexibility of the model, this large ratio could not be explained, and the authors concluded that another mechanism must be producing the effect. Some improvements to the quasifree calculations for ^{4}He were obtained in Ref. [4] by adding a triton knockout amplitude to the proton knockout amplitude,

$$T_{fi}\sim\phi(k_t)f_{\pi p}(\mathbf{k}_\pi,-\mathbf{k}_t,\mathbf{k}'_\pi,\mathbf{k}_p)+\phi(\mathbf{k}_p)f_{\pi t}(\mathbf{k}_\pi,-\mathbf{k}_p,\mathbf{k}'_\pi,\mathbf{k}_t). \quad (1)$$

Allowing the two amplitude to beat against each other, the authors could improve the agreement with measured small ratios at large proton-^{3}H center-of-mass angles. This improved agreement was then assumed to be evidence for direct triton knockout. However, the large ratios at smaller proton-^{3}H center-of-mass angles were unexplained.

In this paper the results of ^{4}He$(\pi,\pi'p)^3$H calculations with the recoil-corrected continuum shell model (RCCSM) [7] are presented. The RCCSM has recently been applied to ^{4}He$(e,e'N)$ and compared with virtually all available data [8]. The calculations demonstrated the importance of employing a realistic model and, in fact, the same model, for both the initial and continuum states. A realistic NN effective interaction, translational invariance, antisymmetry, and coupled spin and charge exchange channels place the RCCSM at the same level of phenomenology as bound-state shell model calculations. Distortion of the outgoing nucleon does not require the ambiguity of an optical model, but results from the same NN interaction that generates the bound states. Tests of the appropriateness of the Michigan-three-Yukawa (M3Y) interaction [9] included ^{3}H$(p,n)^3$He, ^{3}H$(p,p)^3$H, and ^{3}He$(n,n)^3$He cross section, analyzing power, and polarization calculations, which agreed extremely well with data up to $E_N=70$ MeV [2,10].

II. THEORY

The RCCSM wave functions are expanded in harmonic oscillator basis functions of the form

$$\phi^{J_BM_B}_{\alpha nlj}(\xi)=(1-P_{34})/\sqrt{2}\times|Os^{\nu/2}(\xi_1)Os^{2\nu/3}(\xi_2)\chi^{1/2}_\alpha\Phi^{3\nu/4}_{nlj}(\xi_3)\tau_3\rangle^{J_B}_{M_B}, \quad (2)$$

where $\chi^{1/2}_\alpha$ is the ^{3}H or ^{3}He spin wave function. The oscillator constant is taken to be $\nu=0.36$ fm^{-2} to reproduce the charge radius of ^{3}H. Only single-scattering events are considered, and so one is interested in one-body matrix elements of the form

$$\left\langle\phi^{J_B}_{\alpha nlj}(\xi)\right\|\sum_i O(\mathbf{r}'_i,\boldsymbol{\sigma}'_i)\left\|\phi^{J'_B}_{\alpha'n'l'j'}(\xi)\right\rangle, \quad (3)$$

where $\mathbf{r}'_i$ is the position vector of particle i measured from the four-particle center of mass as shown in Fig. 1. The cross section for $(\pi,\pi'p)$ with the triton and proton emerging in definite spin states in the pion-^{4}He center-of-mass system (ACM) is given by

$$\frac{d^3\sigma}{d\Omega_{k'}d\Omega_{p'}d\omega_{k'}}=(2\pi)^4\frac{k'p'\omega'_p\omega'_k\omega_B\omega_k}{kR(\omega_k+\omega_B)}|T_{fi}|^2, \quad (4)$$

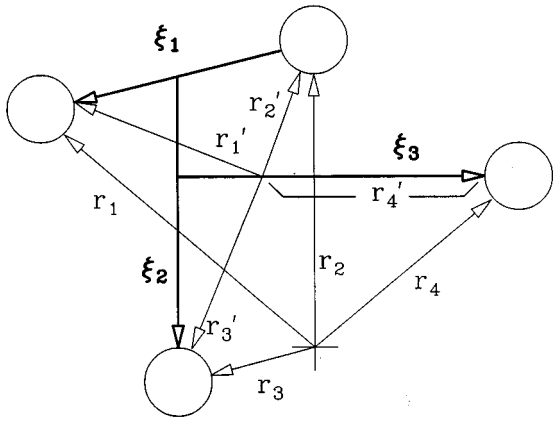

FIG. 1. RCCSM coordinates.

where

$$T_{fi}=\left\langle \psi_{\pi}^{(-)}(\mathbf{r})\psi_{m_S m_A}^{(-)}(\xi)\left|\sum_i \gamma t_c(\pi i)\right|\psi_{\pi}^{(+)}(\mathbf{r})\psi_B(\xi)\right\rangle, \tag{5}$$

and R is the recoil factor $[1+\omega_p'/\omega_A+\omega_p\mathbf{k}'\cdot\mathbf{p}'/(p'^2\omega_A)]$. This process is illustrated in Fig. 2(a) with the coordinate system shown in Fig. 2(b).

The πN t matrix for a particular isospin channel and in the πN center-of-mass system (2c.m.) can be written as

$$t_c=u_1(E_c)+u_2(E_c)k_c^2\cos\theta_c+\nu(E_c)2k_c^2\sin\theta_c(i\boldsymbol{\sigma}\cdot\hat{\mathbf{n}}), \tag{6}$$

where $\hat{\mathbf{n}}=\mathbf{k}_c\times\mathbf{k}_c'/k_c^2$. The center-of-mass energy and momentum, E_c and k_c, are determined in a frozen nucleon approximation. The term $k_c\cos\theta_c$ is approximated by $k^2-q^2/2$, and the term $2k_c^2\sin\theta_c$ $(i\hat{\mathbf{n}}\cdot\boldsymbol{\sigma})$ is approximated by $(k/k_c)(-i\mathbf{q})\times(\mathbf{k}+\mathbf{k}')\cdot\boldsymbol{\sigma}$. The factor γ in Eq. (5) is the usual factor to transform t_c from the 2 c.m. to the ACM. The momentum transfer $\mathbf{q}$ is taken to be $\mathbf{p}-\mathbf{p}'$ and operates on the nuclear coordinates, while $\mathbf{k}$ and $\mathbf{k}'$ operate on the incoming and outgoing pion coordinates. With these approximations, the $(\pi,\pi' p)$ cross section may be calculated with the same form factors as the $(e,e'p)$ cross sections in Ref. [10].

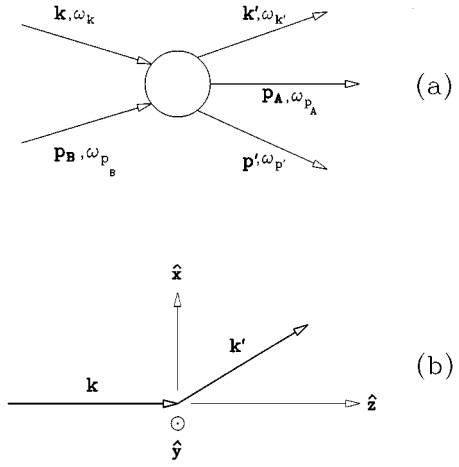

FIG. 2. (a) A schematic of the reaction with k and k' representing the incoming and outgoing pion, p' the outgoing proton, B the index for ^{4}He, and A the index for ^{3}H. (b) The coordinate system employed.

The p-^{3}H wave function with outgoing flux ν_f with final conditions $f=\{\alpha J_A M_A m_s\}$ takes the form [10]

$$\psi_f^{(-)}=(2\pi)^{-3/2}(4\pi/p_f)\sum (i)^l Y_{lm_l}^*(\hat{\mathbf{p}})e^{-i\sigma_l}$$
$$\times(-i/2)C_{m_l m_s m}^{l1/2j}C_{M_A m M_B}^{J_A j J_B}\Psi_c^{J_B M_B(-)}, \tag{7}$$

where the sum is over $lm_l jmJ_BM_B$ and

$$\psi_c^{J_BM_B(-)}=\sum_{c'} r^{-1}u_{c'}^{J_B(-)}(r)|\alpha' J_A' l' j' J_B M_B\rangle. \tag{8}$$

The radial function $u_{c'}^{J_B(-)}(r)$ has the asymptotic form

$$u_{c'}^{J_B(-)}(r)=u_{c'}^{J_B(+)*}\rightarrow(\nu_c/\nu_{c'})^{1/2}(O_{c'}\delta_{c'c}-I_{c'}S_{cc'}^*). \tag{9}$$

The index c stands for $\alpha J_A l j$ with J_A and j coupled to J_B, where J_A is the angular momentum of a possible core state, l and j are the nucleon orbital angular momentum and total angular momentum, respectively, p_f is the nucleon momentum in the nucleon-nucleus center-of-mass frame, and α represents other quantum number necessary to distinguish core states.

The channel states $|\alpha J_A l j(J_B)\rangle$ are linear combinations of the basis states in Eq. (2). A matrix element of a single-particle operator has four matrix elements for each of the four operators O_1, O_2, O_3, and O_4, $\langle D|O_i|D\rangle$, $\langle E|O_i|D\rangle$, $\langle D|O_i|E\rangle$, and $\langle E|O_i|E\rangle$, where $|D\rangle$ and $|E\rangle$ represent the direct and exchange parts of the basis states. When a proton takes the position of particle number 4 in both initial and final states, the terms $\langle D|O_4|D\rangle+\langle E|O_3|E\rangle$ may be associated with a quasifree calculation in that they look like a proton making a transition between single-particle orbits. The other direct terms and the exchange terms are large, and one can see their effect by comparing the ^{4}He(e,e') calculations of Ref. [11], which omitted them and bear no relation to the data, and the calculations of Ref. [10] which included them and agree with the data. The triton knockout amplitude of Eq. (1) was calculated as one would for elastic scattering from a triton and then the recoil of the triton represented by a distorted wave for the relative p-^{3}H motion. It is more difficult to identify terms with this amplitude. It is easier to identify terms which would be missing from the triton knockout amplitude, and these are the exchange terms and channel coupling terms, both of which are large.

The channel wave functions exhibit coupling through the index c', which runs over all channels allowed to connect to the channel c, including the charge exchange channels. The charge exchange strength is determined by the effective NN interaction. This means that neutron excitations contribute to proton knockout. Neutron excitations also contribute to proton knockout through the neutrons in the recoiling ^{3}H, as in the triton knockout model, in terms such as $(\langle D|+\langle E|)|O_1+O_2(|D\rangle+|E\rangle)$.

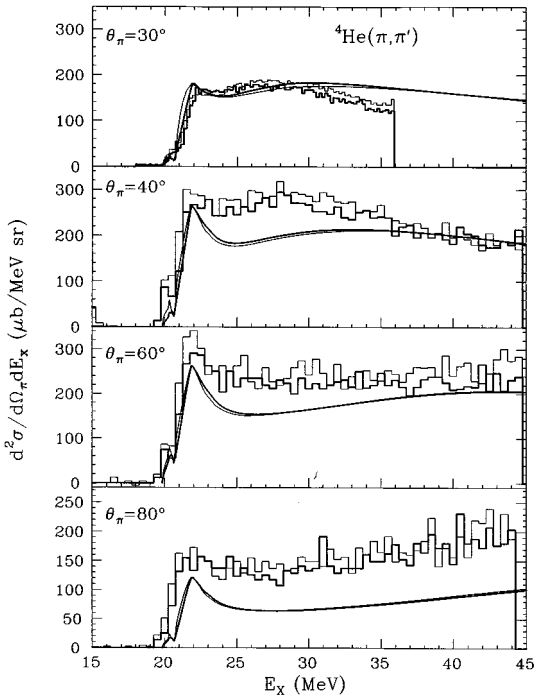

FIG. 3. Inclusive excitation functions. The thick lines are the calculations for $^4\mathrm{He}(\pi^+,\pi^{+\prime})$; the thin lines are for $\mathrm{He}(\pi^-,\pi^{-\prime})$. The histograms represent the data of Refs. [3] and [12].

III. RESULTS

The inclusive calculations at $\theta_\pi^{\mathrm{lab}}=30°$, 40°, 60°, and 80° are shown in Fig. 3 along with the data of Refs. [3] and [12]. The 30° excitation function was calculated previously in Ref. [12] by including only the $\langle D|O_4|D\rangle+\langle E|O_3|E\rangle$ terms and employing a pion distorting potential calculated with the energy shift method of Ref. [13]. As pointed out in Ref. [3], the energy shift method gives a rather poor elastic cross section when compared with the measured elastic cross section. Also pointed out in Refs. [3] and [4] is that different pion potentials, which compare equally well with elastic data, can give inelastic cross sections which differ by factors of 2. The cross sections in Fig. 3 were calculated with the elastic parameters $\lambda=1$, $b_0=(-0.067,0.031)$, $\overline{c_0}=(0.105,0.168)$, $B_0=(0.,0.074)$, and $C_0=(1.829,0)$, in the notation of

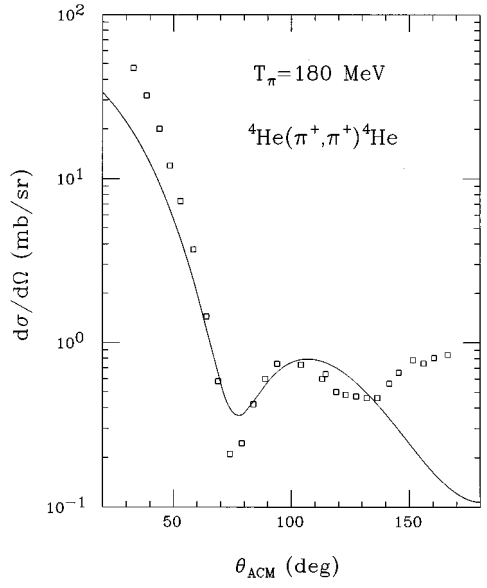

FIG. 4. Calculated elastic cross section and the data of Ref. [15].

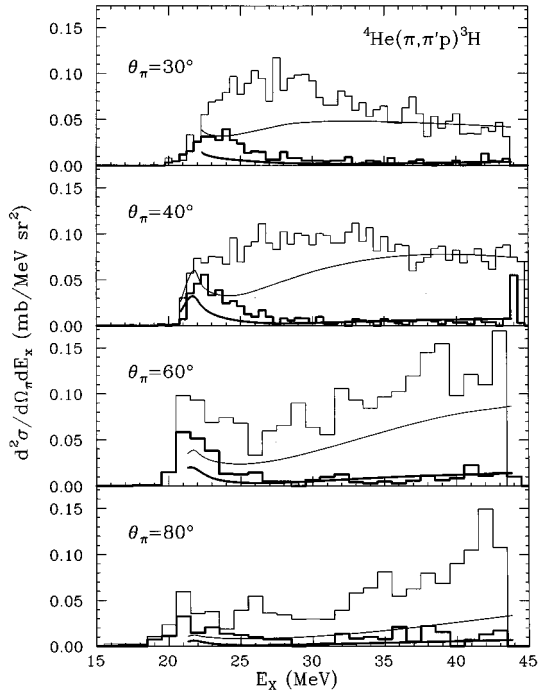

FIG. 5. Exclusive excitations functions, averaged over laboratory proton angles of $\phi_p^{\mathrm{lab}}=180°$ and $\theta_p^{\mathrm{lab}}=30°$, 45°, 60°, 75°, and 90°. The thin lines are the calculations for $^4\mathrm{He}(\pi^+,\pi^{+\prime}p)^3\mathrm{H}$; the thick lines are for $^4\mathrm{He}(\pi^-,\pi^{-\prime}p)^3\mathrm{H}$. The histograms represent the data of Ref. [12].

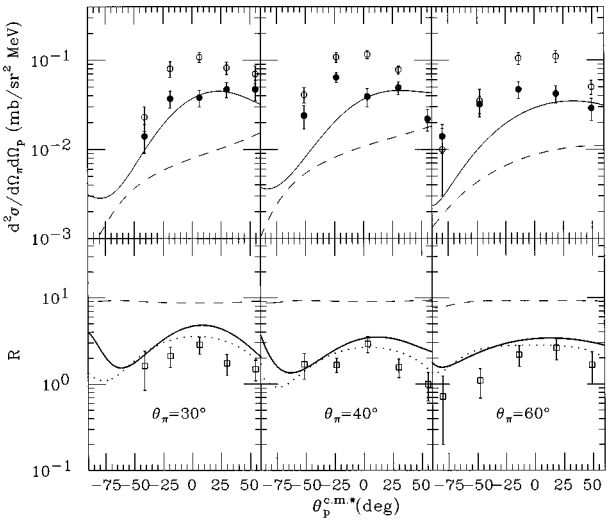

FIG. 6. Top panels are cross sections integrated over $21.5<E_x<25.0$ MeV. Open (solid) circles are π^+ (π^-) data of Ref. [3]; solid (dashed) lines are calculations for π^+ (π^-). Bottom panels are the ratio of π^+ to π^-. Squares are data of Ref. [3]; thick solid lines are complete RCCSM calculations; dashed lines omit neutron form factors; dotted lines omit channels corresponding to $n+^3\mathrm{He}$ from the wave function.

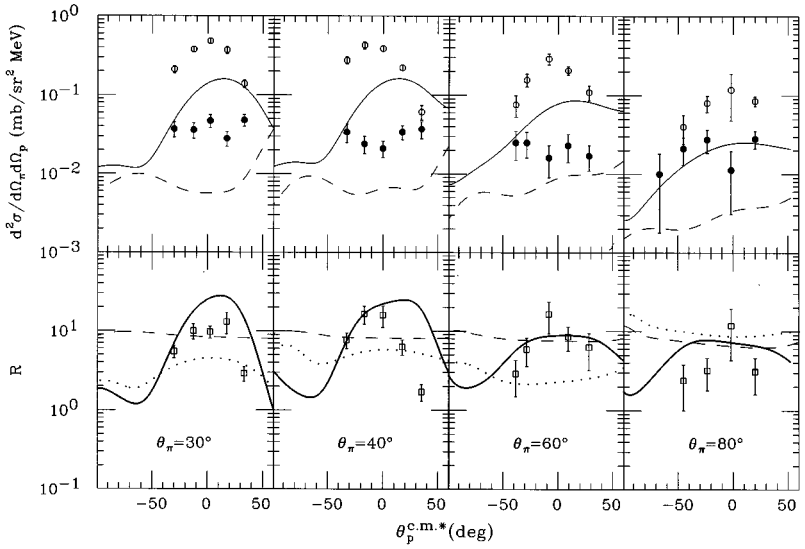

FIG. 7. Top panels are cross sections integrated over $25<E_x<30$ MeV. Open (solid) circles are π^+ (π^-) data of Ref. [3]; solid (dashed) lines are calculations for π^+ (π^-). Bottom panels are the ratio of π^+ to π^-. Squares are data of Ref. [3]; thick solid lines are complete RCCSM calculations; dashed lines omit neutron form factors; dotted lines omit channels corresponding to $n+{}^3$He from the wave function.

Stricker, McManus, and Carr [14]. The parameters are a result of a ten-parameter fit to elastic scattering of π^+ from ^{4}He with T_π ranging from 50 to 180 MeV, and the resulting elastic cross section is shown in Fig. 4 along with the data of Ref. [15]. Many sets of parameters produced a χ^2 as good as those employed here, and the pion-distorting potential remains an ambiguous element of all calculations in this paper. A characteristic of the potentials attempted is that if a reasonable fit is obtained for the 30° data in Fig. 3, the 80° cross sections are small, as in the figure.

Plotted in Fig. 5 are the exclusive $(\pi,\pi' p)$ excitation functions. The cross sections are laboratory cross sections averaged over laboratory proton angles of $\phi_p^{\rm lab}=180°$ and $\theta_p^{\rm lab}=30°$, 45°, 60°, 75°, and 90°. The calculated 30° excitation function shows a weakness in the resonance region that one would not expect from the inclusive results in Fig. 3. This may be due to a normalization difference between the inclusive measurements of Ref. [12] at 30° and those of Ref. [3] at 40°, 60°, and 80°, or it may be that the experimental proton spectrum is more sharply peaked in plane than the calculated spectrum. The calculated spectrum becomes more in plane with increasing excitation energy and, hence, the rising behavior of the calculated exclusive excitation functions.

Angular distributions for the outgoing proton are shown in the upper panels of Figs. 6–9 as a function of the proton

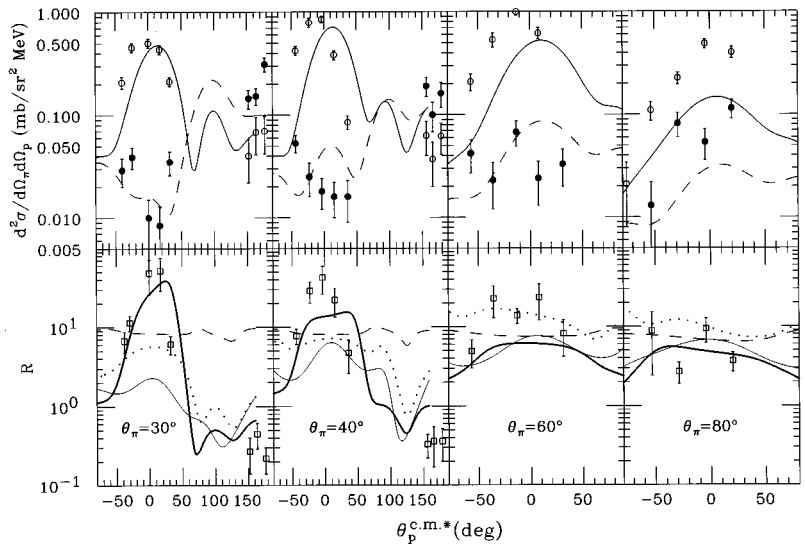

FIG. 8. Top panels are cross sections integrated over $30<E_x<40$ MeV. Open (solid) circles are π^+ (π^-) data of Ref. [3]; solid (dashed) lines are calculations for π^+ (π^-). Bottom panels are the ratio of π^+ to π^-. Squares are data of Ref. [3]; thick solid lines are complete RCCSM calculations; dashed lines omit neutron form factors; dotted lines omit channels corresponding to $n+{}^3$He from the wave function; thin lines omit $J_B'=2^+$ channels.

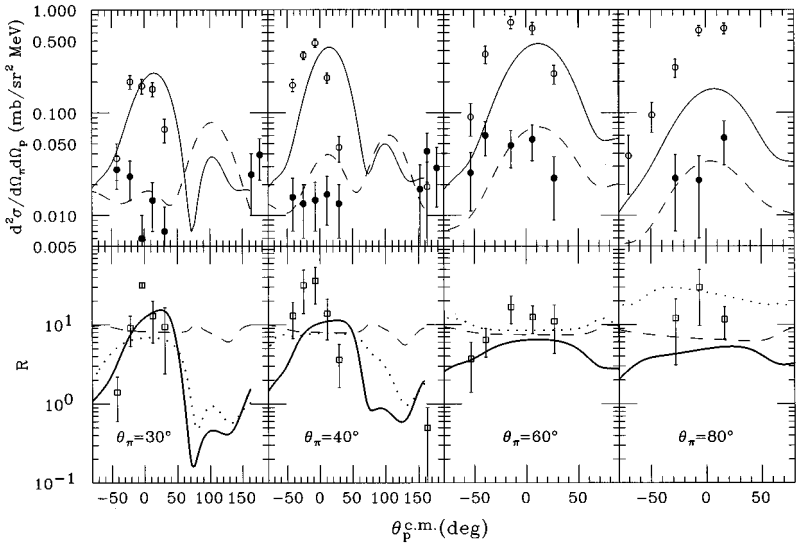

FIG. 9. Top panels are cross sections integrated over $40<E_x<45$ MeV. Open (solid) circles are π^+ (π^-) data of Ref. [3]; solid (dashed) lines are calculations for π^+ (π^-). Bottom panels are the ratio of π^+ to π^-. Squares are data of Ref. [3]; thick solid lines are complete RCCSM calculations; dashed lines omit neutron form factors; dotted lines omit channels corresponding to $n+{}^3$He from the wave function.

angle $\theta_p^{\text{c.m.}}$* measured in the center of mass of the four-nucleon system. Angles are measured from the velocity vector of the four-nucleon system with the positive direction counterclockwise. The experimental cross sections are shown as open circles for π^+ and the solid circles for π^-. The calculated cross sections are $d^2\sigma/d\Omega_{k'}d\Omega_{p_{\text{c.m.}}}$ which are believed to correspond to the experimental cross sections. The solid lines in the upper panels correspond to π^+ and the dashed lines to π^-. As in the excitation function calculations of Fig. 5, the low excitation energy cross sections are too small. The squares in the lower panels are the ratios of π^+ to π^-. The most drastic deviations from the quasifree value of 9 appear in Fig. 8 at $\theta_\pi=30°$ where the cross sections were integrated over the $30<E_x<40$ MeV region and continue in Fig. 9 where the cross sections were integrated over the $40<E_x<45$ MeV region. The thick solid lines in the bottom panels are the calculated π^+ to π^- ratios, and they do a good job of reproducing the experimental values. These calculated ratios are not sensitive to the pion-distorting potentials as were the cross sections.

The dashed lines are the RCCSM calculations with the neutron form factors set to zero, i.e., no charge exchange coupling terms and no contribution from neutrons in ^{3}H. These values are near the quasifree value of 9. Setting the neutron form factors to zero affects the π^+ cross sections only modestly, but produces a large effect on the π^- cross sections. This is, of course, because the π^-n elementary amplitude is 3 times the π^-p in the Δ_{33} resonance region.

The form factors may be broken down in a different manner by eliminating from the final proton wave functions all channels that correspond to a neutron coupled to ^{3}He. Then the only neutrons that contribute to the proton knockout amplitude are those that remain in ^{3}H. This is equivalent to eliminating charge exchange coupling from the wave functions, but not from the Hamiltonian that produced the wave functions.

The resulting calculated ratios are shown as the dotted lines in the bottom panels of Figs. 6–9. These lines do a reasonable job of reproducing the small ratios at large angles, but not the large ratios at small angles, as did the triton knockout model. In the context of the RCCSM, one would not call this evidence for direct triton knockout, but the effect of recoil terms. These are the same recoil terms which give $(+e/2,-e/2)$ for the (proton, neutron) $E1$ effective charge. It is, then, the charge exchange channels which boost the π^+/π^- ratio to high values. The process may be thought of as a π^- hitting a neutron and then the neutron initiating possible collision sequences that result in knocking out a proton. The possibility of charge exchange producing the large π^+ to π^- ratios was mentioned in Ref. [4].

It is difficult to analyze the ratio beyond verification of its

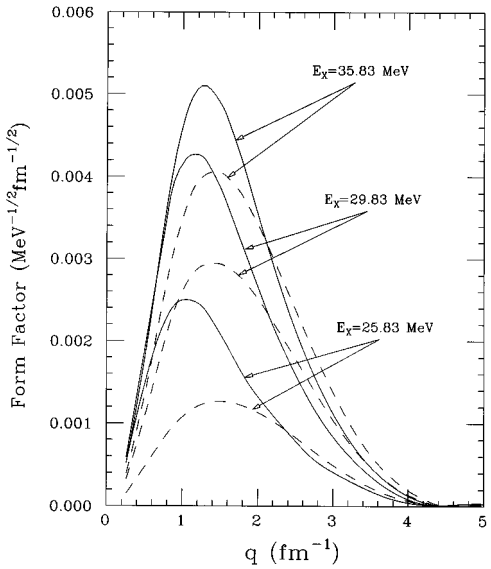

FIG. 10. Solid lines are proton form factors; dashed lines are neutron form factors times a factor of 3.

charge exchange origin. All channels with l less than 4 contribute to some extent. However, the extremely large value in the $30<E_x<40$ MeV region occurs primarily with the addition of the $J_B=2^+$ channels. This is demonstrated in the bottom panel of Fig. 8 with the thin solid line which omits the $J_B=2^+$ channels. The magnitudes of the $J_B=2^+$, $l=2$, and $j=3/2$ neutron and proton form factors, $\langle\psi_c^{J'_B}\|\Sigma_i j_2(qr'_i)Y_2(\hat{\mathbf{r}}'_i)\|\psi_{\text{g.s.}}\rangle$, for $E_x=25$, 30, and 36 MeV are plotted in Fig. 10. Here one can see the rapid increase in the neutron form factors at the $E_x=30$ MeV region. It may be that large π^+/π^- ratios are a signal of regions of increased neutron excitations in a particular channel and, therefore, a signal for giant resonances. In fact, the region of large π^+/π^- ratios in ^{16}O is near $E_x=30$ MeV where the $E2$ strength has been observe via $^{16}\text{O}(\gamma,n_0)^{15}\text{O}$ [16].

IV. CONCLUSION

The primary conclusion of this article is that neutron excitations which couple to the outgoing proton channels are responsible for the extremely large $(\pi^+,\pi^{+\prime}p)/(\pi^-,\pi^{-\prime}p)$ ratio in the $30<E_x<45$ MeV region. However, three additional points can be made. First, agreement with the experimental π^+/π^- ratio was obtained with RCCSM wave functions that also reproduce $^3\text{H}(p,n)^3\text{He}$, $^3\text{H}(p,p)^3\text{H}$, and $^3\text{He}(n,n)^3\text{He}$ cross section, analyzing power, and polarization data and most of the $^4\text{He}(e,e'X)$ data. It was not necessary to invoke any other mechanism other than single scattering with a simple πN t matrix. Therefore, one model is able to provide a connection among many data sets over a large range of continuum nucleon energy. Second, the π^+/π^- ratio becomes large in regions of increasing neutron excitations and may be a signal for giant resonance excitation. Third, measurement of the π^+/π^- ratio has provided tighter restrictions on the charge exchange coupling in the continuum wave functions than electron scattering data, where the neutron couples to the probe only through the anomalous magnetic moment. The charge exchange channel was introduced into the calculations of Ref. [17] via a Lane model in order to improve agreement with $^4\text{He}(e,e'p)$ data, and yet provided a larger contribution than the RCCSM predicted. The π^+/π^- ratios provide an opportunity to test the wave functions employed in this and other calculations.

[1] J. R. Calarco, B. L. Berman, and T. W. Donnelly, Phys. Rev. C **27**, 1866 (1983).
[2] D. Halderson and R. J. Philpott, Phys. Rev. C **28**, 1000 (1983).
[3] M. K. Jones *et al.*, Phys. Rev. C **46**, 52 (1992).
[4] J. Langenbrunner, M. K. Jones, D. Dehnhard, C. L. Morris, and W. R. Gibbs, Phys. Rev. Lett. **69**, 1508 (1992).
[5] L. Rees, N. S. Chant, and P. G. Roos, Phys. Rev. C **26**, 1580 (1982).
[6] T. Takaki and M. Thies, Phys. Rev. C **38**, 2230 (1988).
[7] D. Halderson and R. J. Philpott, Nucl. Phys. **A321**, 295 (1979).
[8] D. Halderson, Phys. Rev. C **53**, 2978 (1996).
[9] G. Bertsch, J. Borysowiez, H. McManus, and W. G. Love, Nucl. Phys. **A284**, 399 (1977), the interaction described on p. 412.
[10] D. Halderson, J. Phys. G **20**, 1461 (1994).
[11] Hotta *et al.*, Phys. Rev. C **38**, 1547 (1988).
[12] C. L. Blilie *et al.*, Phys. Rev. Lett. **57**, 543 (1986).
[13] W. B. Cottingame and D. B. Holtkamp, Phys. Rev. Lett. **45**, 1826 (1980).
[14] K. Stricker, H. McManus, and J. A. Carr, Phys. Rev. C **19**, 929 (1979).
[15] B. Brinkmöller *et al.*, Phys. Rev. C **44**, 2031 (1991).
[16] T. W. Phillips and R. G. Johnson, Phys. Rev. C **20**, 929 (1979).
[17] J. F. J. van den Brand *et al.*, Nucl. Phys. **A534**, 637 (1991).